KSME Journal, Vol. 7, No. 4, pp. 389~398, 1993

A Study on the Combustion Characteristics of Coaxial Jet Furnaces with Swirl Flow

Soon-Yong Shim*, Kang-Ho Sohn and Chang-Sik Lee****

(Received June 26, 1993)

This study is an analysis of the turbulent diffusion flame with swirl flow and the calculated results are compared with experimental data in cases of various swirl numbers and air-fuel ratios. The mathematical model is restricted to single-phase, diffusion controlled combustion with swirl flow. Values of local flow properties are obtained by solving appropriate differential equation for continuity, momentum, stagnation enthalpy, concentration, turbulence energy, dissipation rate of turbulence energy, and the mean square of concentration fluctuation. The method is proposed for calculating the local probability of chemical reaction on the use of the probability density function for the mixture fraction.

Key Words: Swirl Flow, Turbulent Diffusion Flame, Concentration Fluctuation

Nomenclature

AF : Air fuel ratio
C_p : Specific heat
D_f : Diameter of furnace (m)
F : The value of f with a maximum probability
f : Time mean mixture fraction
f' : Fluctuating component of mixture fraction
g : Time mean square of fraction of mixture fraction
i : Stoichiometric mass of oxidant
M : Molecular weight
R : Universal gas constant (=8.314 kJ/kmol)
R_0 : Burner exit radius (m)
SN : Swirl number
S_0 : Source term

Greek letters

α : Proportion of time
Γ_0 : Exchange coefficient for variable ϕ
μ : Effective viscosity ($=\mu_t+\mu_l$)
σ : Variance
σ_f : Effective Schmidt number
ϕ : Extensive property
φ : Vane angle of swirler

Subscripts

A : Condition at the entering unpremixed oxidizer stream
F : Condition at the entering unpremixed fuel stream
fu : Fuel
ox : Oxygen
pr : Products
j : Species
st : Stoichiometric

* GoldStar Industrial Systems Research and Development Lab.
** Department of Mechanical Engineering, Hanyang University

1. Introduction

The turbulent diffusive combustion has drawn much attention because it is considered to be safer and more economical than pre-mixed combustion because it has little probability of explosion and can be realized with a burner which is relatively simple in construction. In spite of these merits, the diffusive combustion is rarely employed in industry because, in high combustion intensity, the flames tend to lift from nozzles and the flame length is too long to be utilized in most cases.

If swirling force is exerted on the combustion

air of turbulent diffusive combustion process, almost of above mentioned problems can be solved because of higher stability of flames and improvement in mixing rate of fuel and oxidizer.

However, the flow field of swirling combustion exhibits very complex patterns, which makes the analysis of swirling combustion very difficult. As a consequence, there were only a few studies on swirling combustion process compared with many studies on unrealistic but easy-to-analyze non-combustion swirl flow in the furnace.

Khalil and Spalding(1975) applied the k-ε turbulent models to the combustion analysis and used eddy-break-up combustion model in which the chemical reaction rate was determined according to the production rate of combustion products. However, there was large discrepancy between their results and experimental data. Eldin(1979) applied the same turbulent models and square wave combustion model in which the fluctuation distribution of combustion products' densities is assumed to take battlement shape, which is an unreasonable assumption(1982), also leading to unsatisfactory results. Elgobashi(1974) drew more acceptable results based on the assumption that the fluctuation distribution of combustion products' densities takes clipped Gaussian shape. However, he used stream function method to analyze flow field instead of directly calculating combustion products' velocities, which leads to some discrepancy between numerical data and experimental data. Other studies (Ramos and Somer, 1985 ; Habib and Whitelaw, 1980) applied k-l turbulent models resulted in less accurate solutions.

In this paper, fluid dynamics and thermodynamics of the combustion with swirl flow in the coaxial furnaces are studied. It is assumed that chemical reaction of fuel and oxidizer determines the spatial distribution of the time-mean densities of combustion products. The k-ε turbulent models with clipped Gaussian combustion model are employed in the analysis of concentrations, densities, velocities, and temperature of combustion products. The velocities of combustion products are directly calculated using the SIMPLER algorithm and thus we obtain better results than Elgobashi did. The results are compared with experimental data.

2. Theoretical Analysis

2.1 Modeling

For analysis of the combustion characteristics, the sudden expansion type furnace was selected as a model of furnace. The vane type swirler was attached at the entrance of combustion chamber as shown in Fig. 1. It was assumed that the temperature of the furnace wall was isothermal. The conservation equations are as follows in axisymmetric cylindrical coordinate.

$$\frac{\partial}{\partial x}[\rho U\phi]+\frac{1}{r}\frac{\partial}{\partial r}[r\rho V\phi] = \frac{\partial}{\partial x}[\Gamma_0\frac{\partial\phi}{\partial x}]+\frac{1}{r}\frac{\partial}{\partial r}[r\Gamma_0\frac{\partial\phi}{\partial r}]+S_0. \quad (1)$$

The extensive properties(ϕ) are listed in Table 1.

In turbulent modeling, following definitions and standard k-ε model was used.

$$-\overline{\rho uv}=\mu_t\left[\frac{\partial U}{\partial y}+\frac{\partial V}{\partial x}\right] : -\overline{\rho uw}=\mu\left[\frac{\partial V}{\partial x}\right], \quad (2)$$

$$\mu_t=\frac{c_D k^2}{\varepsilon}=\mu_{eff}-\mu. \quad (3)$$

The turbulent model constants are listed in Table 2.

2.2 Calculation of temperature and density

The stagnation enthalpy and energy equations are defined as follows.

$$h=m_{fu}H_{fu}+\sum m_j C_{pj}T+\rho[U^2+V^2+W^2], \quad (4)$$

$$\frac{\partial}{\partial x}[\rho Uh]+\frac{1}{r}\frac{\partial}{\partial r}[r\rho Vh]$$

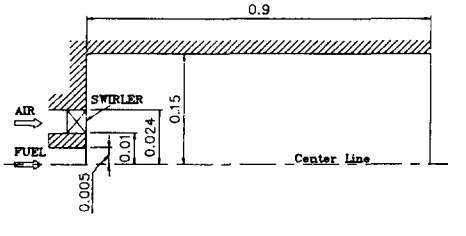

Fig. 1 Schematic diagram of the combustion chamber

Table 1 The form of flow governing equation

ϕ	Γ_0	S_0
1	0	0
U	μ_{eff}	$-\frac{\partial P}{\partial x}+\frac{\partial}{\partial x}[\mu_{eff}\frac{\partial V}{\partial x}]+\frac{1}{r}\frac{\partial}{\partial \gamma}[r\mu_{eff}\frac{\partial V}{\partial x}]$
V	μ_{eff}	$-\frac{\partial P}{\partial r}+\frac{\partial}{\partial x}[\mu_{eff}\frac{\partial U}{\partial x}]+\frac{1}{r}\frac{\partial}{\partial r}[r\ \mu_{eff}\frac{\partial V}{\partial x}]-2\mu_{eff}\frac{V}{r^2}+\frac{\rho W^2}{r}$
Wr	μ_{eff}	$-\frac{2}{r}\frac{\partial}{\partial r}[\mu_{eff}\ Wr]$
k	$\frac{\mu_{eff}}{\sigma_k}$	$G_{k1}-\rho\varepsilon$
ε	$\frac{\mu_{eff}}{\sigma_\varepsilon}$	$\frac{\varepsilon}{k}(C_1G_{k1}-C_2f\rho\varepsilon)$

$$G_{k1}=\mu_{eff}\left[2\left[\left(\frac{\partial U}{\partial x}\right)^2+\left(\frac{\partial V}{\partial r}\right)^2+\left(\frac{V}{r}\right)^2\right]+\left(\frac{\partial W}{\partial x}\right)^2+\left[r\frac{\partial}{\partial r}\left(\frac{W}{r}\right)\right]^2+\left(\frac{\partial U}{\partial r}+\frac{\partial V}{\partial x}\right)\right]$$

$$\frac{\partial}{\partial x}(\rho Uf)+\frac{1}{r}\frac{\partial}{\partial r}(r\rho Vf)=\frac{\partial}{\partial x}\left(\frac{\mu_{eff}}{\sigma_f}\frac{\partial f}{\partial x}\right)+\frac{1}{r}\frac{\partial}{\partial r}\left(r\frac{\mu_{eff}}{\sigma_f}\frac{\partial f}{\partial r}\right)$$

$$\frac{\partial}{\partial x}(\rho Ug)+\frac{1}{r}\frac{\partial}{\partial r}(r\rho Vg)=\frac{\partial}{\partial x}\left(\frac{\mu_{eff}}{\sigma_g}\frac{\partial g}{\partial x}\right)+\frac{1}{r}\frac{\partial}{\partial r}\left(r\frac{\mu_{eff}}{\sigma_g}\frac{\partial g}{\partial r}\right)+C_{g1}G_{g1}-C_{g2}\rho\frac{\varepsilon}{k}$$

$$G_{g1}=\mu_{eff}\left[\left(\frac{\partial f}{\partial x}\right)^2+\left(\frac{\partial f}{\partial r}\right)^2\right]$$

Table 2 Turbulent model constant

σ_k	σ_ε	C_1	C_2
1.0	1.3	1.44	1.92

$$=\frac{\partial}{\partial x}\left[\frac{\mu_{eff}}{\sigma_h}\frac{\partial h}{\partial x}\right]+\frac{1}{r}\frac{\partial}{\partial r}\left[r\frac{\mu_{eff}}{\sigma_h}\frac{\partial h}{\partial r}\right]. \tag{5}$$

Both the kinetic energy of the mean flow and the turbulence are negligible compared to the heat of reaction H_{fu}.

Knowledge of the instantaneous values of the mass fraction and temperature gives the value of the instantaneous density ρ via the perfect gas law.

$$\rho=\frac{P\sum(m_j/M_j)}{RT}$$

The used fuel is propane(C_3H_8) in this analysis, and combustion products are assumed to be O_2, N_2, and H_2O.

2.3 The chemical reaction model

(1) Model assumption

(a) The turbulent transport coefficients for the two reactants are equal at every point in the field.

(b) 1 kg of fuel always combines with (i) kg of oxidizer to produce ($1+i$)kg of combustion products.

(c) The fuel and oxidizer may coexist at the same place but at different times.

(d) The reaction is infinitely fast.

2.4 The model for concentration fluctuations

The mixture fraction, for calculating mass fraction of each component, is defined as follow

$$f=\frac{(m_{fu}-m_{ox}/i)_M-(m_{fu}-m_{ox}/i)_A}{(m_{fu}-m_{ox}/i)_F-(m_{fu}-m_{ox}/i)_A}. \tag{7}$$

In order to obtain the time mean value, θ, of a statistically-steady, randomly fluctuating quantity $\tilde{\theta}$(t), varying with time, one needs information about its probability density function $P(\tilde{\theta})$ which may be defined through

$$P(\tilde{\theta})\Delta\tilde{\theta}=\lim_{t\to\infty}\frac{1}{t}\sum(\Delta t) \tag{8}$$

$\tilde{\theta}$: Fluctuation,

θ : Time mean value,

$P(\tilde{\theta})$: Probability density function,

$$\int_{-\infty}^{\infty} P(\tilde{\theta})\, d\tilde{\theta}=1. \tag{9}$$

From the knowledge of $P(\tilde{\theta})$ the time mean value θ can be obtained from the definition

$$\theta=\int_{-\infty}^{\infty} \tilde{\theta} P(\tilde{\theta})\, d\tilde{\theta}. \tag{10}$$

Here, the clipped Gaussian distribution is selected as the probability density function. Two parameters are required to specify the probability density function. The first is the mean value f, and the other is the mean square departure from the mean value or the variance, g, which is defined as

$$g=(\tilde{f}-f)^2=f'^2. \tag{11}$$

The forms of conservation terms and equations for f, g are listed in Table 1.

(1) The clipped Gaussian distribution

Followings are definition of clipped Gaussian distribution and the process of evaluating time mean properties.

$$P(\tilde{f})=\exp\left[\frac{-(\tilde{f}-f)^2}{2\sigma^2}\right][U(\tilde{f}-0)-U(\tilde{f}-1)]/\frac{\sigma}{\sqrt{2\pi}} +2A_0\delta(\tilde{f}-0)+2A_1\delta(\tilde{f}-1). \tag{12}$$

Here, $U(\xi)$ is heaviside step function ($U(\xi)=0$, $\xi<0$; $(\xi)=1$, $\xi>0$) and $\delta(\xi)$ is Dirac delta function. A_0 and A_1 represent the integration of the probability density function from the negative infinity to zero, and from 1 to the positive infinity respectively.

The time mean value, f, and the variance, g, of $P(\tilde{f})$ are respectively given by the first moment about $\tilde{f}=0$ and the second moment about the mean value of the area under $P(\tilde{f})$ (Khalil, 1982).

Evaluation of time-mean properties

$$m_{fu}=m_{fu,1}A_1+\int_{f_{st}}^{1}\left(\frac{\tilde{f}-f_{st}}{1-f_{st}}\right) \exp\left[\frac{-(\tilde{f}-F)^2}{2\sigma^2}\right]\frac{d\tilde{f}}{\sigma\sqrt{2\pi}}, \tag{13}$$

$$m_{ox}=m_{ox,0}A_0+\int_{0}^{f_{st}}\left(1-\frac{\tilde{f}}{f}\right) \exp\left[\frac{-(\tilde{f}-F)^2}{2\sigma^2}\right]\frac{d\tilde{f}}{\sigma\sqrt{2\pi}}, \tag{14}$$

$$m_{pr}=1-m_{ox}-m_{fu}, \tag{15}$$

$$T=A_0T_0+A_1T_1+\int_0^1[(\tilde{h}-\tilde{m}_{fu}H_{fu})/\sum_j\tilde{m}_jC_{pj}], \exp\left[\frac{-(\tilde{f}-F)^2}{2\sigma^2}\right]\frac{d\tilde{f}}{\sigma\sqrt{2\pi}}, \tag{16}$$

$$\rho=A_0\rho_0+A_1\rho_1+\frac{P}{R}\int_0^1[1/\tilde{T}(\sum_j\tilde{m}_j/M_j)] \exp\left[\frac{-(\tilde{f}-F)^2}{2\sigma^2}\right]\frac{d\tilde{f}}{\sigma\sqrt{2\pi}}. \tag{17}$$

It is required too much time for numerical simulation using the clipped Gaussian distribution in calculating above variables. Therefore, in first, the battlement shape distribution was adopted to converge the values of variables. Afterward, these values and experimental data were compared to examine the validity of initial guess values in numerical procedure of clipped Gaussian.

(2) Battlement shape distribution

When it is assumed that the mass fraction is distributed in battlement shape, and α is the time proportion of the maximum and minimum fluctuation components, the time mean mass fraction values of these can be calculated from the assumption of instantaneous reaction between fuel and air (Eldin, 1979).

$$m_{fu}=\alpha\cdot m_{fu+}+(1-\alpha)\cdot m_{fu-}, \tag{18}$$

$$m_{ox}=\alpha\cdot m_{ox}+(1-\alpha)\cdot m_{ox-}. \tag{19}$$

The time mean mass fraction values of other components (CO_2, H_2O, N_2) can be calculated from the number of atom conservation law.

2.5 Boundary conditions

In swirling free jets or flames, both axial flux of the angular momentum G_w and the axial thrust are conserved. Since both these momentum fluxes can be considered to be characteristic of the aerodynamic behavior of the jet, a nondimensional criterion based on these quantities was recommended as a criterion of swirl intensity as

$$SN=\frac{G_w}{G_x\cdot(d/2)}, \tag{20}$$

$$G_w=2\pi\rho U_0^2\frac{R_0^3-R_h^3}{3}\tan\varphi, \tag{21}$$

$$G_x=2\pi\rho U_0^2(R_0^2-R_h^2). \tag{22}$$

It was assumed that initial velocity of entrance, U_{in} constant, and the value of turbulent kinetic energy and turbulent dissipation rate was ass-

umed 0.03 U_{in}^2, 0.1 k^2 respectively. The assumption that the values of dependent variables, ϕ, didn't change in radial direction was adopted, i.e., $\frac{\partial \phi}{\partial r}=0$. Neumann condition, $\frac{\partial \phi}{\partial x}=0$, was used at the exit of furnace. And for accurate calculation near the wall, the wall function was adopted using the following non-dimensional numbers (Nallasamy, 1986).

$$y^+=y\frac{C_D^{1/4}k_p^{1/2}}{\nu}, \quad u^+=u\frac{C_D^{1/4}k_p^{1/2}}{\tau_w}. \tag{23}$$

$$T^+=\frac{(T-T_w)\rho C_p C_D^{1/4}k_p^{1/2}}{q_w}, \tag{24}$$

2.6 Numerical procedures

To obtain discretized equations from the governing equations, the control volume formation method was adopted, and the solution of the discretized equation was obtained by SIMPLER algorithm. The grid formation for calculation is 70×30(axial$\times$radial).

3. Experimental Apparatus and Procedures

Figure 2 illustrates schematically the experimental apparatus. This can be divided into three sections, i.e., fuel and air supply system, combustion chamber, and measuring system. Propane gas was fed from gas tank and air was supplied by turbo fan which is controlled by inverter. Vane angle of swirler was 30°(SN=0.4), 45°(SN=0.7), 60°(SN=1.2) respectively. The combustion chamber is a cylindrical annular tube 300 mm in diameter and 900 mm high. The wall of furnace can be cooled down by coolant for constant wall temperature. The probe is able to enter the tube through the slit at the wall. Both air flow meter and fuel flow meter are the variable area floating type flow meter. Density and friction coefficient were modified on the basis 300 K of temperature. The R-type thermo-couple is inserted in two-hole ceramic pipe that is fixed to the probe in which coolant can flow. And the probe is installed in x-y table that is controlled by DC servo motors and controllers. Thus, mean and fluctuating temperatures of flame were obtained by R-type thermo-couple. Measuring point of flame is controlled by three-dimensional traversing system having a positioning precision of better than 1 mm.

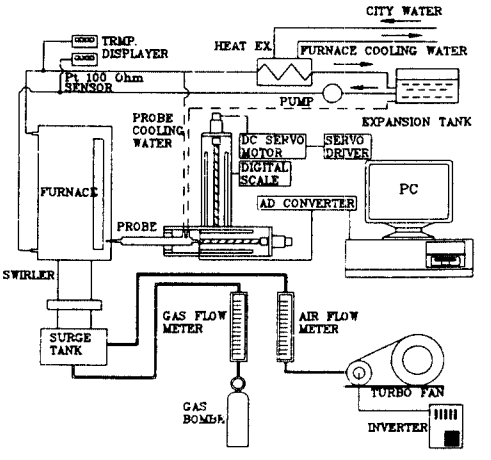

Fig. 2 Schematic diagram of the expreimetal apparatus

The experimental measurement was conducted at three swirl number of 0.4, 0.7, and 1.2. The mean temperature of flame was measured using a water-cooled thermo-couple probe. On the assumption that it was come to the steady state when the flame was stable and the inlet-outlet temperature of coolant was constant, the measuring was set about. The mean temperature was regarded as arithmetic mean of 80,000 data.

4. Results and Discussion

Figures 3, 4 show the calculated mean temperature in combustion chamber and compared with the experimental data in condition swirl number is 0.4 and 0.7 when air-fuel ratio is 23.87(equivalence ratio is 1). The temperature rising takes place late compared with the experiment result near the entrance, but agrees well qualitatively. This error may stem from the assumption that the air velocity of nozzle exit is uniform, and the resistance by swirler is negligible.

Of course, because the hypothesis of k-ε turbulent models is isotropic of fluid flow, the numerical solution may be drawn with some errors, especially near the exit of nozzle. Furthermore, when swirl number becomes higher, the calculation results may have more discrepancy with

reality. We can see, however, that the characteristics of combustion in furnace are able to predicted using k-ε turbulent models and probability density function from Figs. 3 and 4. When the clipped Gaussian distribution was adopted, the result was better than in case of the battlement shape distribution. On the other hand, it requires 15 times calculation time in simulation, the economic factors might be considered. For example, when exact data of combustion products is needed, the clipped Gaussian distribution is useful, but the battlement shape distribution may be adopted in order to know the characteristics of the flames.

Owing to swirl effect, the back flow of flame around the center line of the furnace was detected, and in case of swirl number=1.2 (vane angle=60°) the swirl effect was so big that the flames couldn't be hold because it collided with the entrance furnace wall. This phenomenon was predicted from the stream lines of the numerical result.

4.1 Effects of swirl number

The temperature distribution in center line of furnace in case of each swirl number was represented in Fig. 5. Results of computation coincided with experimental data qualitatively and when swirl number was 0.7, the results were more similar than in case of swirl number=0.4. In the first place, it was expected that the numerical results would be coincident with experimental data in case of low swirl number, but the results in that case had more discrepancy with experiment owing to effect of non-uniform inlet air velocity etc. All the more, the results in case of high swirl number showed closer values.

When swirl number was higher than 0.7, the highest temperature of symmetry line appeared in the region which was nearer than X/Df=0.5. This means that the flame length will be shorter with increment of swirl number. As swirl number

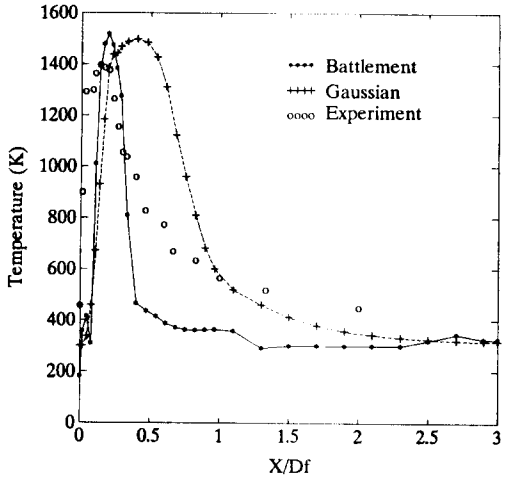

Fig. 3 Distribution of mean temperature (at R=0, SN=0.4)

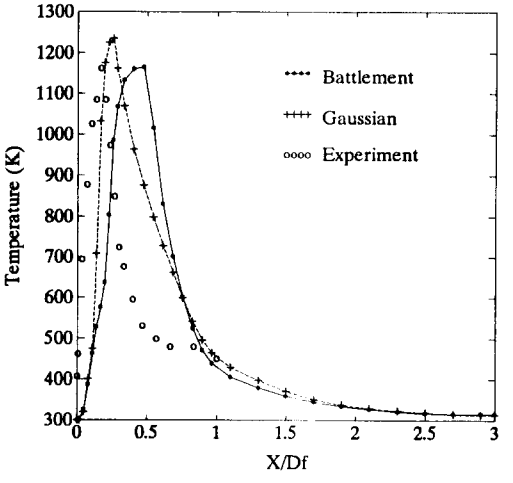

Fig. 4 Distribution of mean temperature (at R=0, SN=0.7)

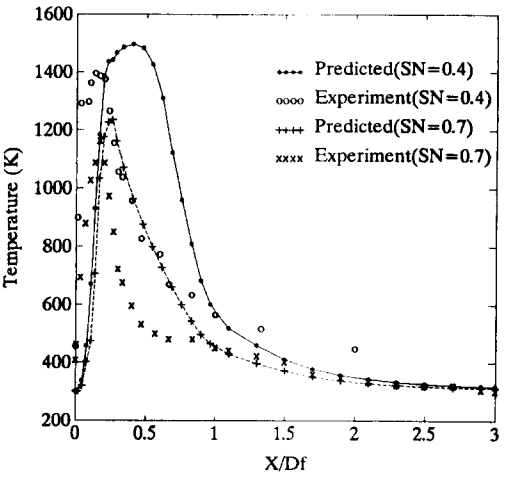

Fig. 5 Distribution of mean temperature (at R=0, AF=25.87)

increases, the flame is more diffusive than that of small swirl number to radial direction and the shape of flame is formed like a vessel. These aspects are illustrated in Fig. 7 which shows the isothermal lines in the furnace. It is a flame sheet where the intervals between lines are dense, and we can see that the flames collide with the entrance wall in case of swirl number = 1.2, Figure 6 represents the temperature distribution at different air-fuel ratio, it exhibits the same tendency with former case.

4.2 Effects of air-fuel ratio on temperature distribution

Figure 8 shows the distribution of temperature with variation of air-fuel ratio. According to the increase of air-fuel ratio, the temperatures at the center line decrease. Of course, because of exceed

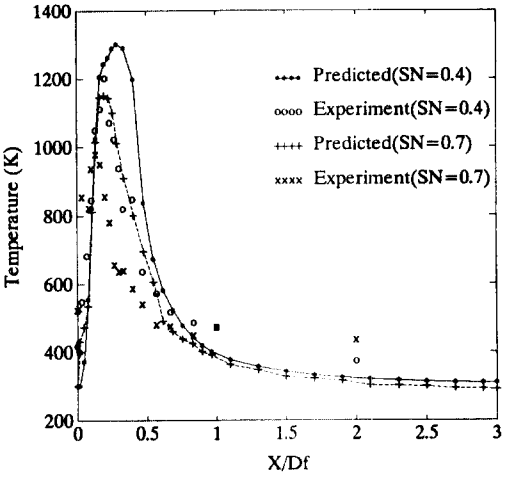

Fig. 6 Distribution of mean temperature (at R=0, AF=35.01)

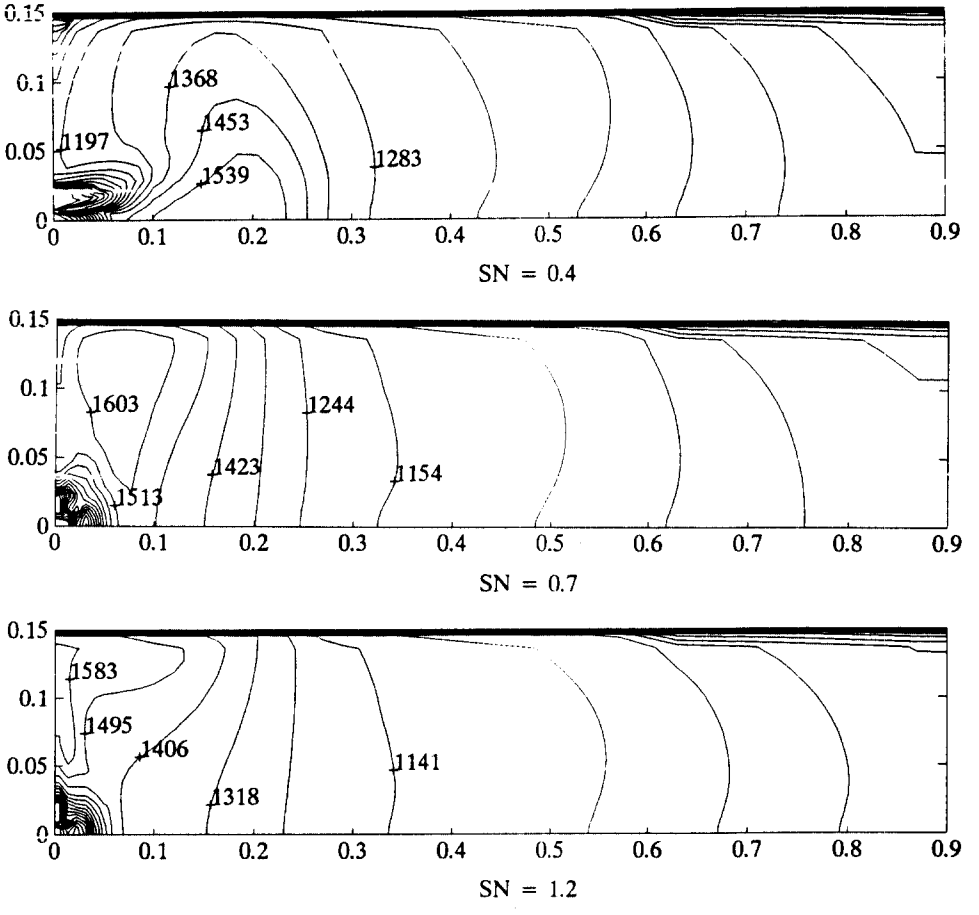

Fig. 7 Isothermal line of flow with variation of swirl number

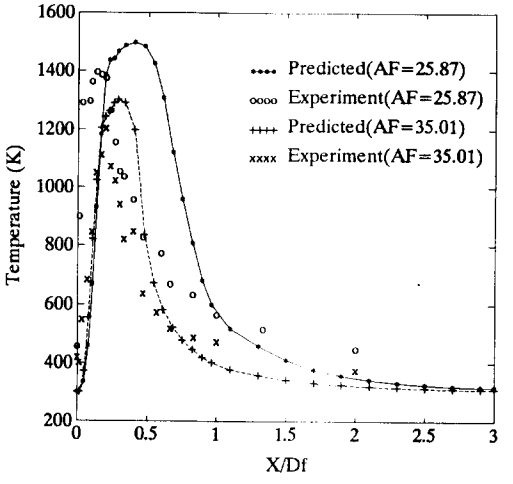

Fig. 8 Distribution of mean temperature (at R=0, SN=0.4)

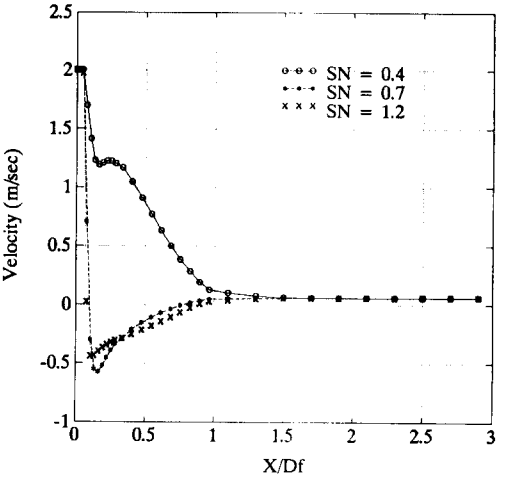

Fig. 9 Distribution of axial velocity (at R=0, AF=25.87)

air which was not involved in reaction with fuel, the temperature was low on the whole in case of high air-fuel ratio. However, as illustrated, the calculated temperature distribution in case of low air-fuel ratio had a tendency to shift from the nozzle to the combustion chamber slightly as in case of low swirl number. On the other hand, in case of high air-fuel ratio, the results agreed well with experimental data quantitatively except the region which is near to the nozzle exit. From that, it can be said that our numerical analysis is able to be employed in case of strong turbulent flow field with better accuracy. This reason may be thought, as previously mentioned, that in case of weak swirl flow the analysis based on assumption of uniform air velocities near the nozzle might have some discrepancy with reality owing to flow resistance by swirler or air-inlet duct, but when strong swirling force is exerted the turbulent intensity is so big that we can neglect the variety of velocities at the exit of nozzle.

4.3 Effects of swirl number on velocity distribution

The axial velocity distribution of combustion field in furnace was plotted in Fig. 9. We can see that in case of weak swirl(swirl number <0.6) the velocity becomes slow down suddenly at exit of nozzle, and increase temporarily by a effect of axial momentum of air flow at X/Df=0.2. In case

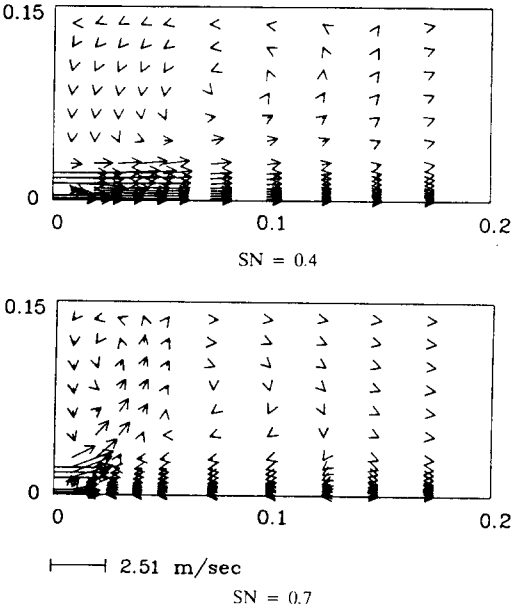

Fig. 10 Vector distribution of velocities near the entrance

of strong swirl, the axial velocity showed the negative values at the points nearer than X/Df= 0.5 When swirl number became strong swirl, the maximum velocity values decreased but the range of negative values expanded to downstream.

It means that the domain of mixing is enlarged, and mixing of fuel and air is accelerated. This

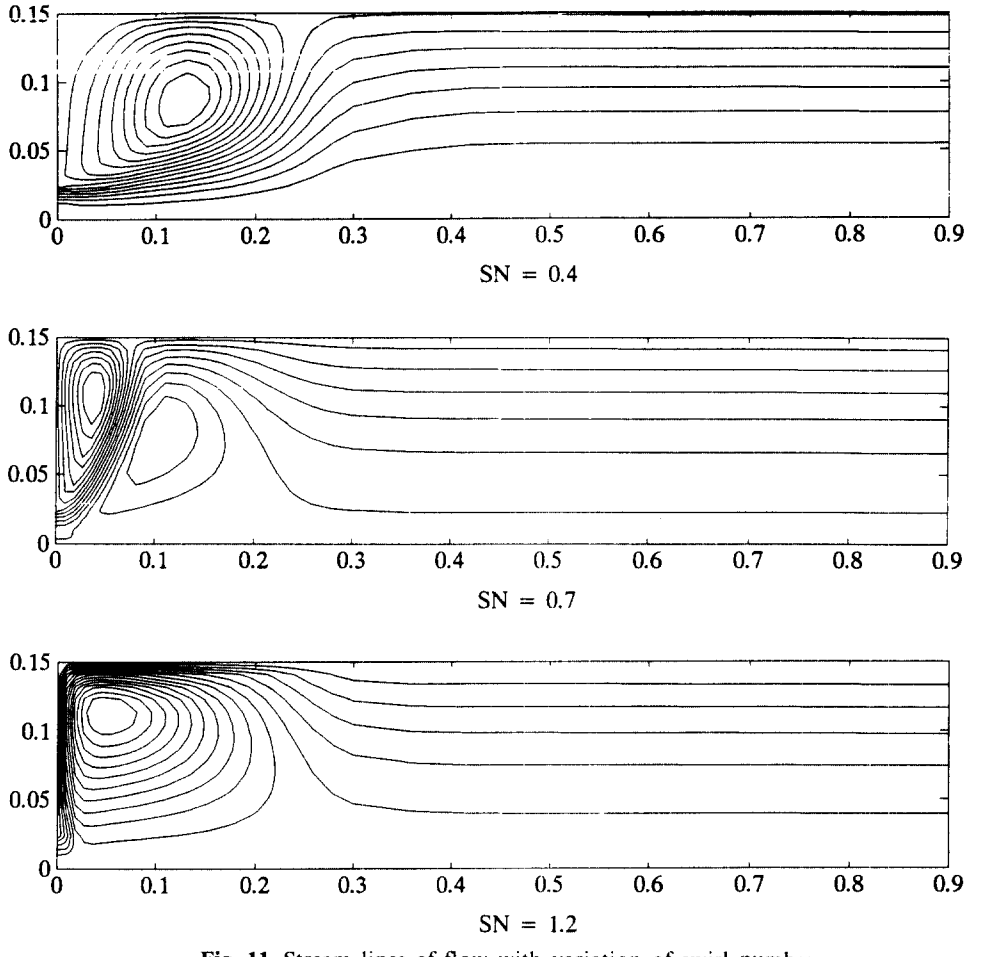

Fig. 11 Stream lines of flow with variation of swirl number

effect plays a important role, i.e., the burned high temperature gas returns back to the nozzle and the entered gas(air and fuel) is preheated, therefore, the reaction is activated near the nozzle. The influence of swirl number on the velocity vectors in furnace is shown in Fig. 10. The vectors distribution of velocities near the entrance show that the increase of swirl number brings about the back flows near the nozzle exit. Figure 11 illustrates the stream lines according to various swirl number in chamber. As strength of swirl increases, the size of recirculation region decreases and we can see the back flow in case of swirl number=0.7 near the center line and the recirculation flow disappears in swirl number=1.2 It can be explained that the flames is formed at the

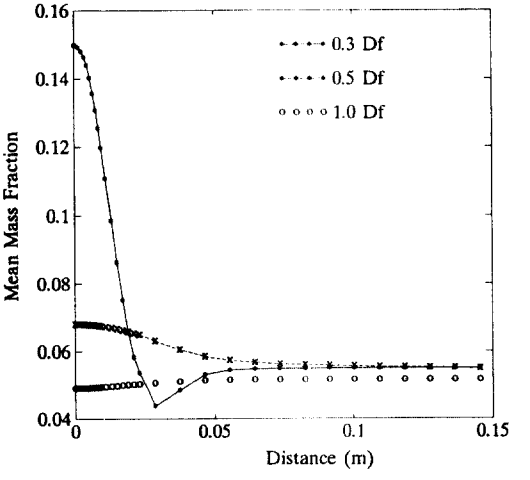

Fig. 12 Radial profiles of mean mixture fraction =0.4)

near area of entrance wall and collide with wall. Therefore the flames are extinguished.

4.4 Distribution of mass fraction

Figure 12 gives the distribution of mean mass fraction along the radius. We can see that the area before X=0.3 Df has big values of mass fraction, on the other hand, there is a few changes in downstream. It means that the real mixing occurs after X=0.3 Df in case of SN=0.4. Considering the temperature distribution and values of mass fraction, it can be said that the mixing of fuel and oxidizer take place at the point slightly before X=0.3 Df. From that we might say the eddies which was made by swirler vane may accelerated the mixing between fuel and oxidizer in reality. And if swirl number was increased, the mixing region became closer to the nozzle.

5. Conclusions

The numerical results and experimental data were compared in order to verify the validity of the numerical analysis using probability density function. The following conclusions may be drawn from the comparison.

(1) When k-ε turbulent models and probability density function was adopted in combustion model, the results appeared to be reasonable, and useful enough to predict the characteristics of combustion in the furnace.

(2) When swirl number was low, the effects of non-uniform velocity and eddies by swirler vane at the nozzle exit played important role in mixing of fuel and oxidizer.

(3) In case of high air-fuel ratio, the temperatures of around center line had a tendency of decrease owing to excess air, and in that case the numerical results coincided well with those of experiment quantitatively except nozzle exit region.

(4) If strong swirl flows were exerted on, the velocity of furnace center line showed the negative values, and as the swirl number, gets higher the wider back flow fields appeared.

References

Djilali, N., Garshore, I. and Salcudean, M., 1989, "Calculation of Convective Heat Transfer in Recirculating Turbulent Flow Using Various Near-Wall Turbulence Models," Numerical Heat Transfer, Part A, Vol. 16, pp. 189~212.

Eldin, M. A. and Spalding, D. B., 1979, "Computation of Three Dimensional Gas Turbine Combustion Chamber Flows," Journal of Engineering for Power, Vol. 101, pp. 327~336.

Elgobashi, S. E., 1974, "Characteristics of Gaseous Turbulent Diffusion Flames in Cylindrical Furnace," Ph.D. Thesis, London University.

Habib, M. A. and Whitelaw, J. H., 1980, "Velocity Characteristics of Confined Coaxial Jets with and without Swirl," Journal of Fluids Engineering, Vol.102, pp. 47~53.

Khalil, E. E., Spalding, D. B. and Whitelaw, J. H., 1975, "The Calculation of Local Flow Properties in Two Dimensional Furnace," Int. Journal Heat and Mass Transfer, Vol. 18, pp.775~791.

Khalil, E. E., 1982, "Modeling of Furnaces and Combustors," Abacus Press.

Launder, E. and Spalding, D. B., 1974, "The Numerical Computation of Turbulent Flows," Computer Methods in Applied Mechanics in Engineering, pp. 269~289.

Nallasamy, M., 1986, "Turbulence Models and their Applications to the Prediction of Internal Flows," Computers and Fluids, Vol. 15, pp. 151~194.

North American Mfg. Co., 1989, "North American Combustion Handbook."

Ramos, J. I., 1983, "Turbulent Nonreacting Swirling Flows," AIAA Journal, Vol. 22, pp. 846~848.

Ramos, J. I. and Somer, H. T., 1985, "Swirling Flows in a Research Combustor," AIAA Journal Vol. 23, pp. 241~248.